

Seismic analysis of a masonry cross vault through shaking table tests: the case study of the Dey Mosque in Algiers

Michela Rossi^{*1a}, Chiara Calderini^{1b}, Ivan Roselli^{2a}, Marialuisa Mongelli^{2a},
Gerardo De Canio^{2a} and Sergio Lagomarsino^{1c}

¹Department of Civil, Chemical and Environmental Engineering, University of Genoa, Via Montallegro 1, 16145 Genoa

²ENEA – Italian National Agency for New Technologies, Energy and Sustainable Economic Development,
Via Anguillarese 301, 00123, Rome, Italy

(Received October 9, 2018, Revised July 26, 2019, Accepted September 27, 2019)

Abstract. This paper presents the results of a monodirectional shaking table test on a full-scale unreinforced masonry cross vault characterized by asymmetric boundary conditions. The specimen represents a vault of the mosque of Dey in Algiers (Algeria), reproducing in detail the mechanical characteristics of masonry, and the constructive details including the presence of some peculiar wooden logs placed within the vault's abutments. The vault was tested with and without the presence of two steel bars which connect two opposite sides of the vault. The dynamic behaviour of both the vault's configurations were studied by using an incremental dynamic analysis up to the collapse of the vault without the steel bars. The use of an innovative high-resolution 3D optical system allowed measure displacement data of the cross vault during the shake table tests. The experimental results were analysed in terms of evolution of damage mechanisms, and in-plane and out-of-plane deformations. Moreover, the dynamic properties of the structure were investigated by means of an experimental modal analysis.

Keywords: masonry cross vault; seismic response; shaking table; collapse mechanism; modal analysis

1. Introduction

The severe seismic damages and collapse of historical masonry buildings experienced in several earthquakes all over the world have highlighted the vulnerability of these structures. Among the different damage mechanisms, those affecting vaulted structures are recurrent. The understanding of vaults collapse mechanisms is fundamental to prevent damages to architectural and artistic assets and to save human lives. Moreover, as the vaults are common floor types of historical masonry buildings, the knowledge of their strength, stiffness and ductility is crucial for analysing the behaviour of the whole building (Rossi *et al.* 2016).

Many studies dealing with the analysis of masonry arches and vaults are based on the modern theory of limit analysis developed by Heyman (1966, 1995). The basic conditions of the theorem's application are that masonry is a material with infinite compressive strength, it has negligible tensile resistance, and no sliding occurs. Therefore, their failure is mainly related to the geometry of the structures and it is caused by loss of equilibrium. A thorough literature of limit analysis methods is provided by Huerta (2004, 2008) and Boothby (2001). Although the knowledge of masonry arch behaviour is rather developed, the complex

3D geometry of masonry vaults makes the study of their structural behaviour more difficult to be analysed. This challenging issue have been recently faced developing 3D graphical and analytical limit analysis methods (O'Dwyer 1999, Block *et al.* 2006, Andreu *et al.* 2007, Baratta and Corbi 2010, Fraternali 2010, Tomasoni and D'Ayala 2011, Angelillo *et al.* 2013, Block and Lachauer 2014), and finite element models (Lourenco *et al.* 1997, Creazza *et al.* 2002, Calderini and Lagomarsino 2004, Szolomicki 2009, Milani *et al.* 2008, Li and Atamturktur 2014). These studies, however, have been mainly addressed to linear and non-linear static analysis, while there is a lack of understanding of the seismic behaviour of masonry vaults. Recent research (Rafiee *et al.* 2008, Van Mele *et al.* 2012, McInerney and DeJong 2015, Caddemi *et al.* 2015) has proved the efficacy of discrete element methods in modelling the heterogeneous nature of masonry structures and in performing dynamic analysis with a reasonable computational effort. However, there is still a need for experimental data to assess the reliability of discrete element modelling approaches in simulating the complex 3D behaviour of masonry vaults. Few experimental studies have actually been carried out in both static and dynamic field. Some authors (Shapiro 2012, Quinonez *et al.* 2010, Van Mele *et al.* 2012, Rossi *et al.* 2016, 2017, Calvo Barentin *et al.* 2017) studied the 3D collapse mechanisms of vaults by testing 3D printed small-scale mock-ups under both supports displacements and loads. Ceradini (1996) analysed a full-scale brick cross vault and a full-scale of a tuff cloister vault.

The first mock-up, which represented a church nave's vault with a span of 7.36 m, was tested by applying an

*Corresponding author, Ph.D.

E-mail: michela.rossi@dicca.unige.it

^aPh.D.

^bAssociate Professor

^cFull Professor

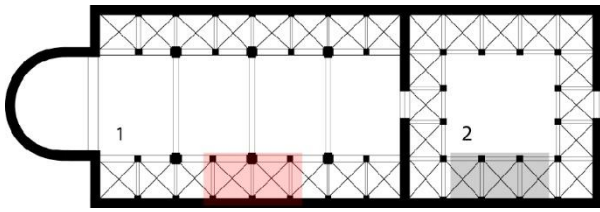


Fig. 1 Example of a typical case of cross vaults with asymmetric boundary conditions in a three naves church (1) with an annexed cloister (2)

outwards movement of two supports until cracks appeared. The tuff cloister vault was tested under uniform loads. Subsequently, two frontal supports were allowed to move progressively outwards because of the vault's thrust. Both the mock-ups were tested again, after their repairing. Theodossopoulos *et al.* (2002) analysed a 1:4 scale mock-up of a cross vault made of wooden blocks and mortar joints under dead load. The area of the vault's diagonals (groins) were then strengthened and the vault tested using the same loading conditions. In Theodossopoulos *et al.* (2016) a 1:15 scale model of a pointed barrel vault made in plaster was subjected to symmetric and asymmetric horizontal spread and the cracks development monitored. Fewer studies focused on the dynamic behaviour of vaults. Ramaglia *et al.* (2016) performed shaking table tests on a full-scale model of barrel vault. Similarly, Giamundo *et al.* (2016) tested a barrel vault in both unreinforced and reinforced conditions. Other researchers (Atamturktur *et al.* 2009, Conte *et al.* 2011) investigated the dynamic behaviour of vaults by means of in-situ dynamic tests for their dynamic characterization.

This paper focuses on the study of the seismic behaviour of unreinforced masonry cross vaults, which are typical covering of churches aisles, and floors of porticos. The plan in Fig. 1 shows two typical examples of cross vaults found in churches aisles and porticos. In this context, cross vaults are frequently characterized by asymmetric boundary conditions and a relevant difference in stiffness between the supports, which are walls on one side, and arcades on the other side. The general purposes of the paper are to study the dynamic behaviour of masonry cross vaults with asymmetric boundary conditions and to identify their main collapse mechanism. The study was carried out by testing a full-scale model of a masonry cross vault on a shaking table. The mock-up represented a vault of the Mosque of Dey in the Citadel of Algiers.

2. Description of the vault's prototype

The Mosque of Dey was the private mosque of the king of Algiers built inside the Palace of the Dey. The palace was located in the Citadel of Algiers that was erected as a refuge and headquarter since the Ottoman occupation (16th century). During the 16th and 19th centuries, the palace passed through several construction phases that unfortunately are not well known.

The plan and the section of the mosque are shown in Figs. 2(a)-(b), respectively. Ten cross vaults and five small

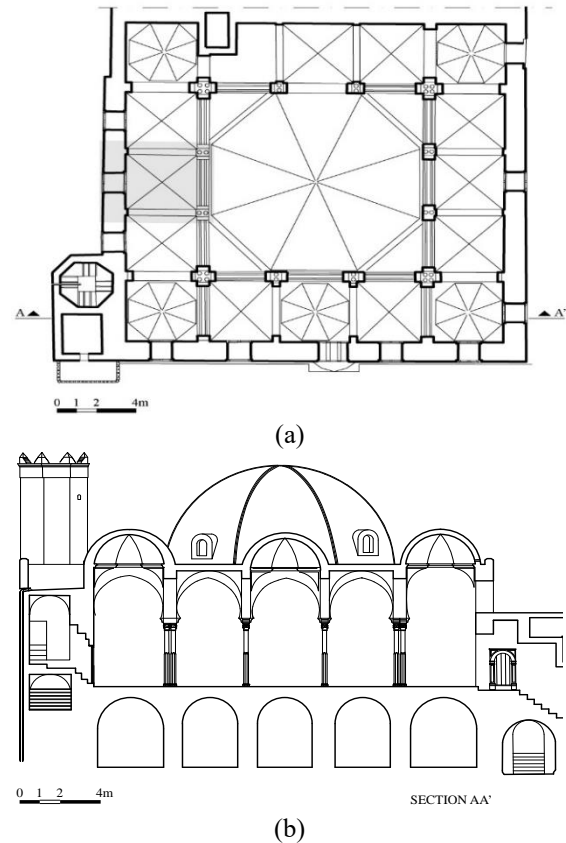


Fig. 2 Plan (a) and section AA' (b) of the Mosque of Dey. In grey, the vault's prototype considered for the design of the full-scale mock-up

domes run along the 20 m square perimeter of the mosque. The cross vaults were supported, on one side by a 36 cm thick external wall, and, on the other side, by marble columns, causing a significant relative stiffness between the two opposite sides. The columns also support a set of pointed arches that define a central area covered by an octagonal dome. All the vaulted structures are made of fired clay bricks assembled with lime mortar.

The cross vault prototype taken as reference for designing the full-scale model is that indicated in grey in Fig. 2(a). A picture of the structure is shown in Fig. 3(a). The plan and the sections of the prototype are illustrated in Figs. 3(b)-(d). The cross vault is one brick layer in thickness. It has an almost square plan ($3.50 \times 3.60 \text{ m}^2$) and a semicircular directrix. Its total height is around 5.65 m. The pointed arch is reinforced by a couple of wooden ties, shown in Fig. 4(a). An interesting constructive detail is the insertion of wood logs of *Thuya*, a typical wood of the Atlas mountain region, between the vault's springing and the column. As shown in Fig. 4(b), the wood elements are arranged in three layers perpendicular to each other and each made of three logs. Some studies (Abdessemed-Foufa 2012, Abdessemed-Foufa *et al.* 2015) mention that this constructive technique was used as a seismic isolator system during post-earthquakes reconstructions of historical buildings in various Algerian cities. The same system was used beneath columns of other buildings of the Citadel, as shown in Fig. 4(c).

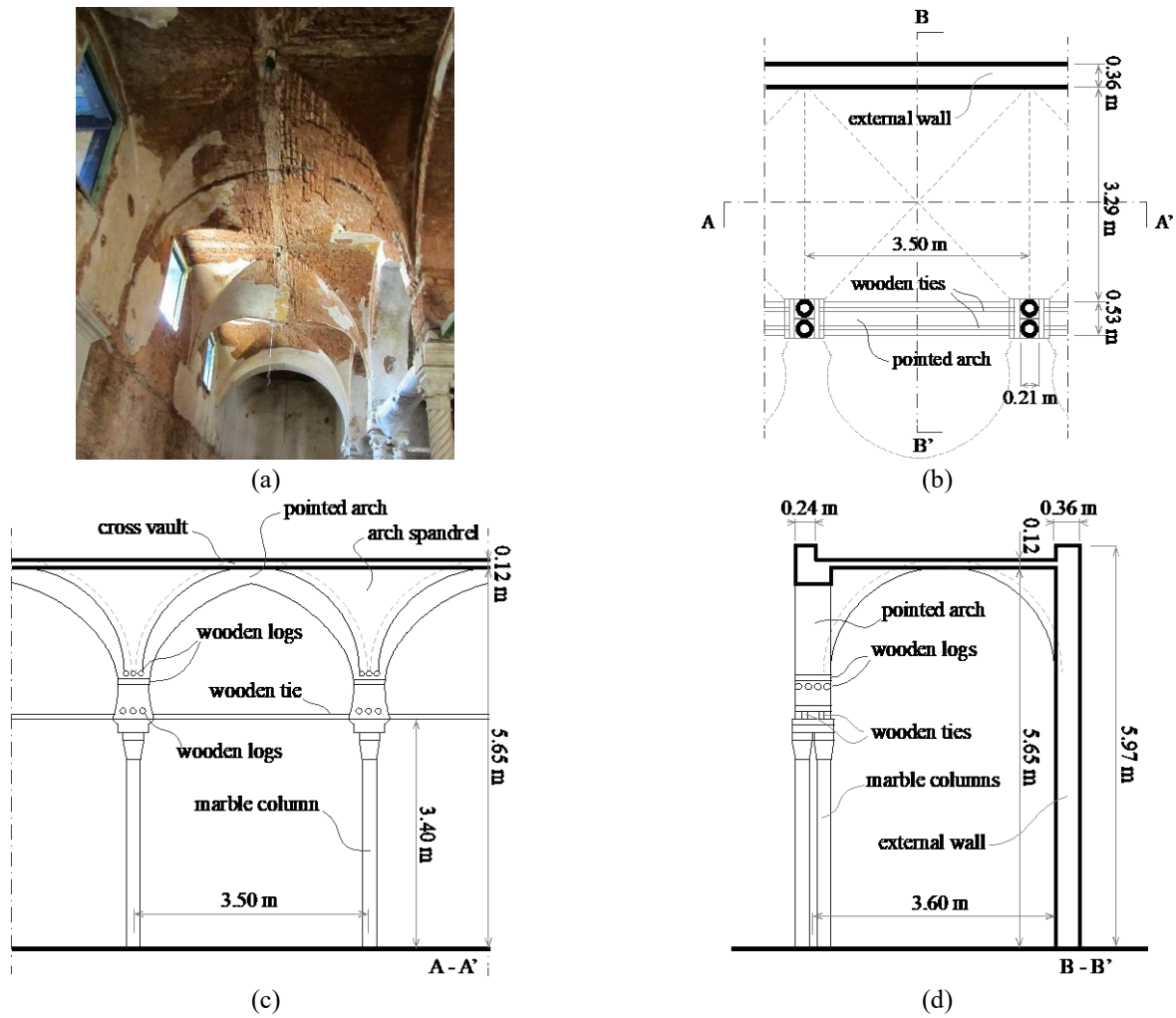


Fig. 3 Vault's prototype for designing the full-scale mock-up (a); plan (b), sections A-A' (c) and B-B' (d) of the cross vault's prototype

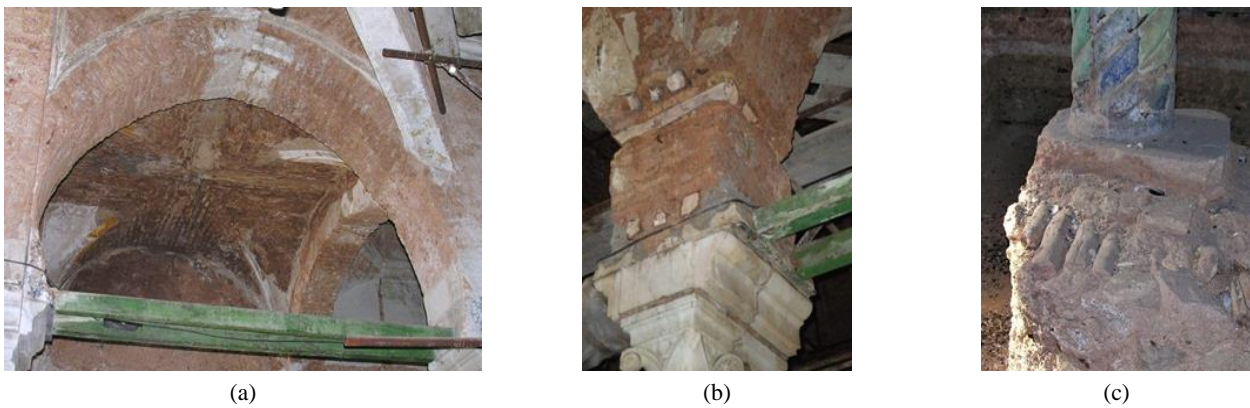


Fig. 4 Pointed arch reinforced with a couple of wooden tie (a); constructive technique of the wooden logs at the arches springing (b); wooden logs at the base of a column of one building of the Citadel (c)

Traditional earth bricks with lime and earth mortar joints with poor mechanical characteristics were used to build both the walls and the vaults. The bricks long side is around 25÷35 cm, while their height is usually modest (around 3÷3.5 cm). On the contrary, mortar joints are rather thick, having more or less the same dimension of bricks' height or even more.

3. Design of the full-scale masonry vault's model

The design of the full-scale model was done studying carefully the geometry of the structure, the stereotomy of the blocks, mechanical characteristics of materials, boundary conditions, and constructive details. Some special measures were taken to meet requirements and limitation

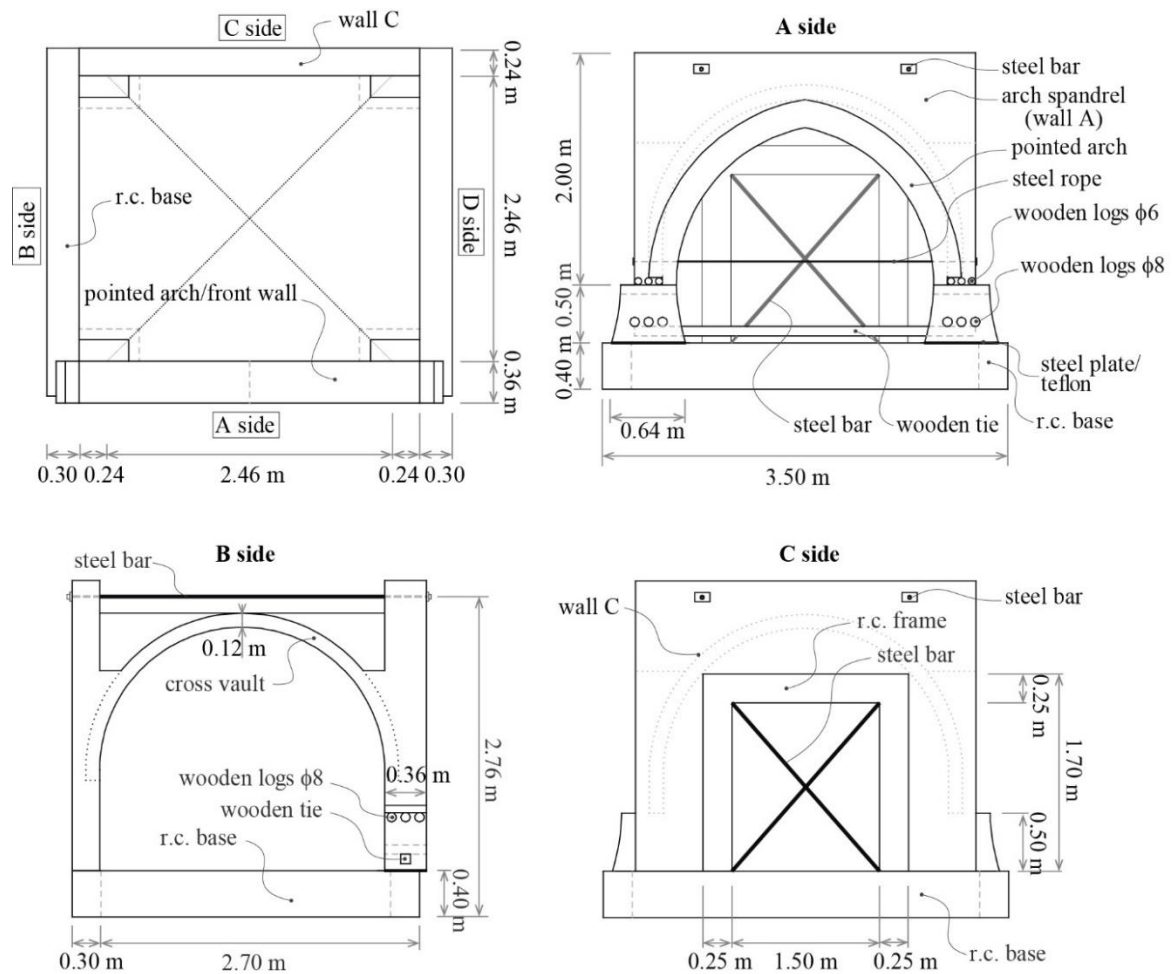


Fig. 5 Design of the full-scale mock-up: plan and elevations

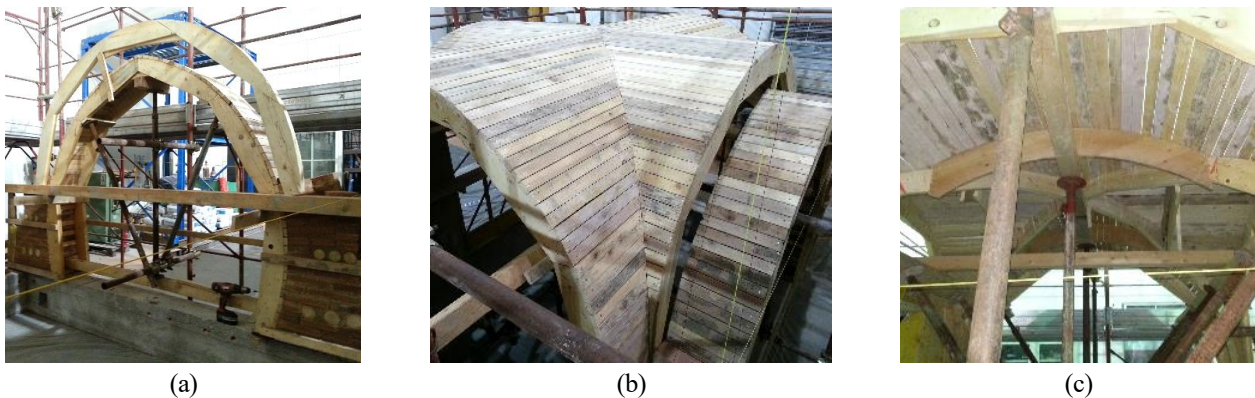


Fig. 6 Wooden scaffolding of the pointed arch (a); view of the masonry cross vault's scaffolding from the top (b) and bottom (c)

that will be explained in the present section.

3.1 Geometry

The full-scale model of the cross vault was built at the shaking table laboratory of the ENEA Casaccia Research Centre in Rome. Overall dimensions and details of the vault were obtained from the technical drawings shown in Figs. 3-4 and from direct observations of the structure. However,

some changes of the geometry had to be done on the basis of technical limitations of the experimental setup and of the shaking table characteristics. Compared to the vault's prototype, the plan of the physical model was smaller ($3.00 \times 3.00 \text{ m}^2$) and it was 2.20 m in height. The mock-up was built over a reinforced concrete frame $3.50 \times 3.00 \text{ m}^2$ in plan. The frame aimed to move more easily the vault from the place where it was built over the shaking table. Fig. 5 shows the plan and the elevations of the 0.12 m thick vault.

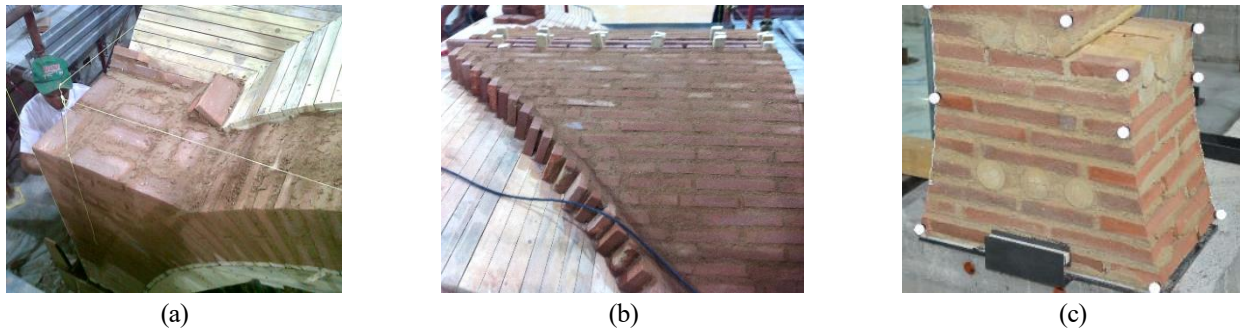


Fig. 7 Building of the vault's support within the thickness of the arch spandrel (a); detail of the bricks arrangement along the cross vault's diagonals (b); detail of the abutment (c)

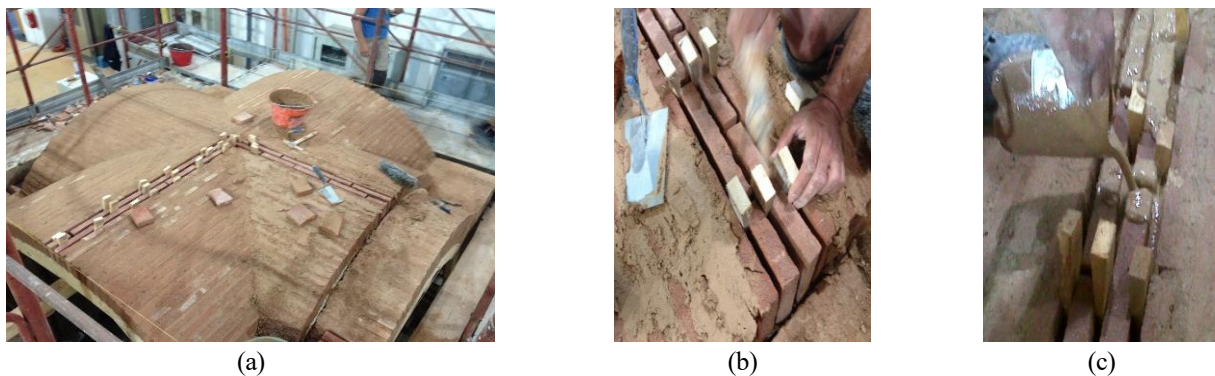


Fig. 8 Positioning of the last bricks in the key of the vault's web (a); stressing of the key bricks using wooden shims (b); pouring of the space between bricks with liquid mortar (c)

The marble columns were not built as their influence on the dynamic response of the vault wanted to be avoided. Moreover, reducing the model's height meant a significant weight reduction that was needed to not exceed the limit of the table (10 tons, see more detail in Section 5). However, the structures had still to be lightened by substituting a portion of the masonry wall with a reinforced concrete frame with two steel diagonal bracing to restore the original stiffness. On the side A, the two abutments, supporting both a 0.24 m thick pointed arch and the vault, were linked by a wooden tie of section 0.08×0.08 m². The geometry and features of the abutments, such as dimensions and arrangement of the wooden logs, replicated as accurately as possible the real ones. The logs placed orthogonal to the side A were 0.08 m in diameter, while the others were 0.06 m. The four corner supports of the cross vault were built, on the side A, within the arch spandrel, while, on the side C, within the thickness of the wall. On the contrary, the edge of the vault's webs was not interlocked with the spandrel and the wall, but it was just placed side by side to them.

The vault's model was tested with and without the presence of two steel longitudinal bars that link the wall C with the arch spandrel (hereinafter called wall A). The two models were called vault with ties (WT) and vault no ties (NT) hereinafter.

3.2 Material

The characteristics of masonry intended to simulate a masonry with weak joints similar to the Algerian masonry.

Regarding the bricks, fired clay bricks of size $0.035 \times 0.12 \times 0.25$ m³ were used, while the joints were around 0.25 m thick. Physical and mechanical characteristics of mortar were established based on available data of the historical Algerian mortar. The mortar elements were clay, small pieces of bricks, gravel, sand, lime, and pozzolana. The final mechanical properties were determined by performing compression and three-point bending tests, according to UNI EN 1015-11:2007 indications. The final compression strength f_m was equal to 3.74 MPa, and the tensile strength τ_m equal to 1.18 MPa. In order to characterize the mechanical properties of masonry, both a triplet and a prism, built assembling clay bricks of size $0.035 \times 0.12 \times 0.25$ m³ and the mortar, were tested. The masonry joint's shear strength determined from the triplet test was 0.015 MPa. The compression test was performed on a masonry prism of $0.25 \times 0.25 \times 0.50$ m³. The value of the compressive strength was of 4.4 MPa and elastic modulus of 327 MPa.

3.3 Building process and boundary conditions

The model was built on a reinforced concrete frame that was moved on the shaking table once the vaulted structure was entirely built. Huge efforts and accuracy were required to build the wooden scaffolding and supporting structures.

The supporting structure used to build the pointed arch is shown in Fig. 6(a), while Figs. 6(b)-(c) illustrate the cross vault's scaffolding from the top and the bottom, respectively. Fig. 7(a) shows the building process of the

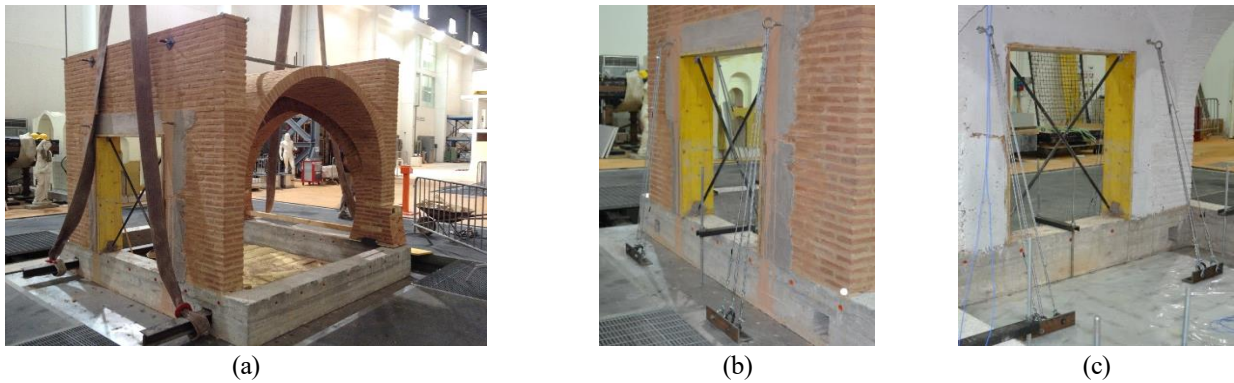


Fig. 9 Moving of the vaulted structure from the building place to the shaking table (a); steel strand cables placed at both sides of the r.c. frame built within the wall C

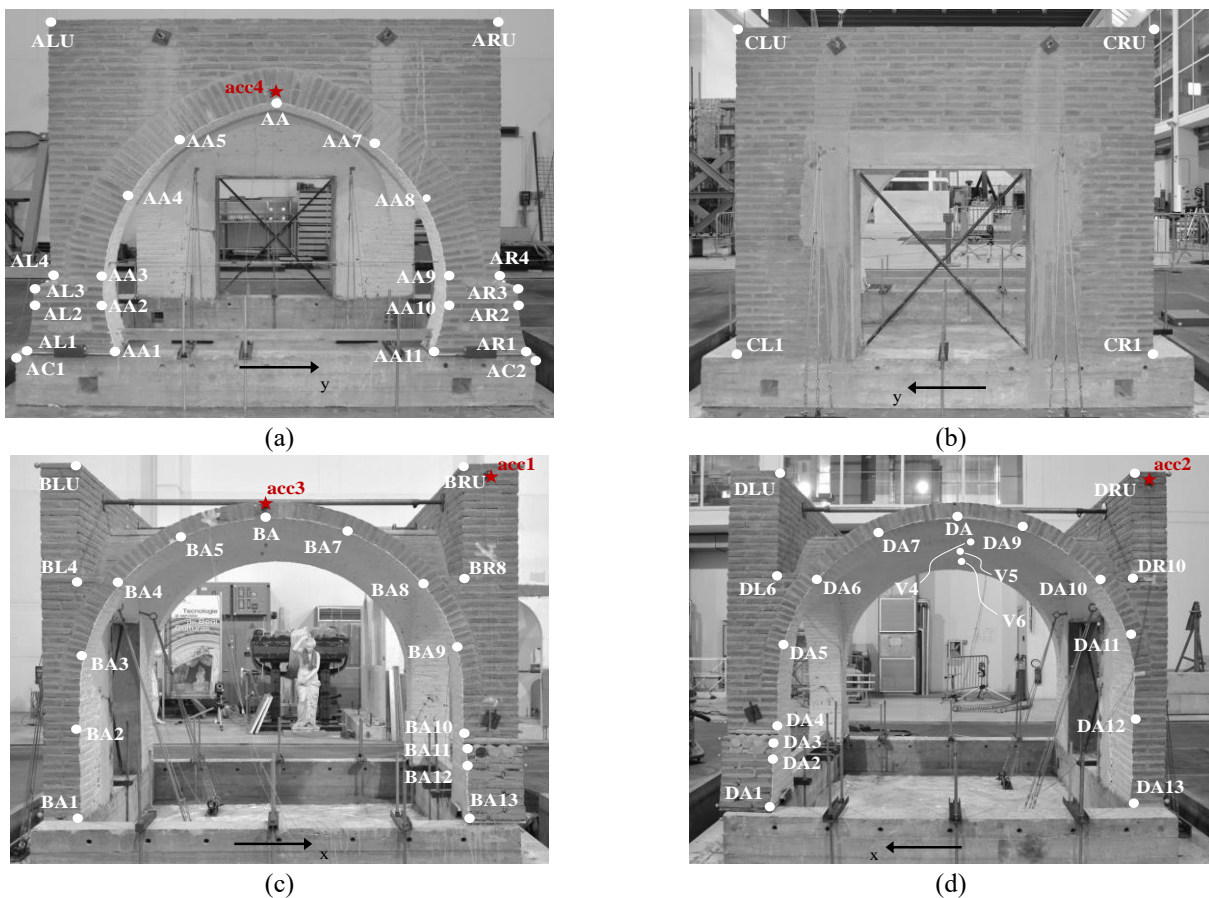


Fig. 10 Identification of the markers and the accelerometers in (a) side A, (b) side C, (c) side B and (d) side D

vault's supports that consisted in building them within the thickness of the arch spandrel. The same thing was done in the opposite side where the supports were built within the walls thickness. On the contrary, the rest of the vault (from the springing to the key) was completely disconnected from both the wall and the arch spandrel, being simply built close to each other. Particularly attention was paid in arranging bricks along the diagonals. Bricks were cut appropriately, studying ancient master builders' solutions observed in historical cross vaults and described in previous works (Gurrieri 1999, Cangi 2005), to allow the interlocking between the vault's webs (Fig. 7(b)). Fig. 7(c) shows the

abutment with the wooden logs. The abutments were built on Teflon sheets so that they could slide in y , while their x displacement was prevented by a steel element. On the opposite side, the reinforced concrete frame was built and the masonry wall erected. The final building step was the "locking" of the vault with key blocks (Figs. 8(a)-(c)). The key bricks were placed in the middle of each vault's webs and then, they were stressed by means of wooden shims, as shown in Fig. 8(b). After this, a liquid mortar was poured through the joints (Fig. 8(c)). Once the mortar dried, the vault acquired its stability and it could transfer loads to its supports. Two steel longitudinal bars not pre-tightened were

Table 1 Specifications of the shaking table

Dimension [m]	4×4	
Degree of Freedom	6	
Frequency range [Hz]	0 - 50	
Max velocity [m/s]	0.78	
Max acceleration [m/s^2]	harmonic	49
	impulse	78
Max displacement [mm]	250	
Mass of tested object [tons]	10	

placed at the top of the structure allowing for the possibility of easily being removed.

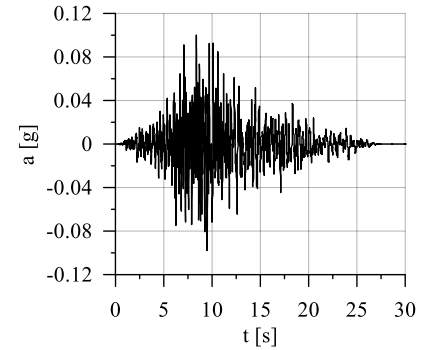
The vault's mock-up was later moved from the place where it was built to the shaking table using a harness system, as shown in Fig. 9(a). In order to prevent deformations of the wall C (and consequently of the whole structure) in x, a system of steel strand cables was anchored to the ground on both side of the masonry wall C (Figs. 9(b)-(c)).

4. Shaking table tests

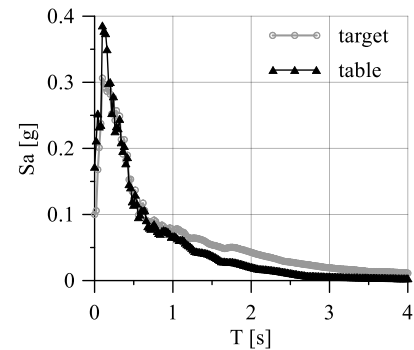
4.1 Testing setup

The dynamic tests were performed at the ENEA Casaccia Research Centre in Rome. The shaking table was a 6-degree of freedom system of size 4×4 m and the maximum specimen mass was 10 tons. The shaking table specifications are indicated in Table 1. Beside traditional accelerometers, the data were acquired from an innovative high-resolution 3D optical system, named 3DVision and tests were remotely shared within the DySCo (Structural Dynamic, numerical Simulation qualification tests and vibration Control) virtual laboratory (De Canio *et al.* 2013, 2016). The displacement data of the cross vault during the shake table tests have been acquired by the ENEA light-based displacement monitoring system provided with 9 near infrared (NIR) digital cameras (De Canio *et al.* 2016). Up to 67 spherical wireless retro-reflecting markers have been applied at selected points of the vault (see Figs. 10(a)-(d)) to reflect the NIR radiation of the cameras. Four DV camera were also used to record synchronized movies. Moreover, the 3D-motion can be monitoring in real-time using a graphical interface that link time histories of the tracked markers with CAD drawings of the structure. Markers were coded with two letters: the first one is A, B, C or D corresponding to the name of the vault's side; the second letter is A, R or L that indicates the markers on arches, those on their right, and those on their left, respectively.

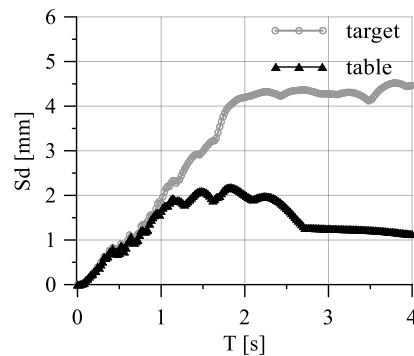
The shaking table was equipped with a 3-axial accelerometer (acc0) to measure the actual input applied to the table. Further 3-axial accelerometers were placed at the top of the wall A (acc1, Fig. 10(c)), at the top of the wall (acc2 in Fig. 10(d)), at the key of the arch of the side B (acc3, in Fig. 10(c)), and at the key of the pointed arch (acc4, in Fig. 10(a)).



(a)



(b)



(c)

Fig. 11 Target acceleration time history (a); comparison between the acceleration (b) and displacement response spectra (c) of the target input and the input actually measured on the table on sequence Rnd_1

4.2 Input acceleration

Tests were performed by applying the North-South component of the ground motion registered during the 21 May 2003 Keddara earthquake (ked_NS) along y direction. The target acceleration time history is shown in Fig. 11(a). Figs. 11(b)-(c) show the target acceleration and the displacement response spectra, respectively, compared with the response spectra of the input actually measured on the table. The signal was normalised and rescaled to the site of the Citadel of Algiers according to the uniform hazard response spectrum (UHRS). Tests were performed at increasing value of Peak Ground Acceleration (PGA) of 0.05 g. The actual acceleration applied to the table, named Peak Table Acceleration (PTA), was measured with the accelerator acc0.

Table 2 Set of acceleration input considered for testing the vault WT

Sequence	PGA [g]	PTA[g]	Damage
Rnd_1	0.01	-	characterization
ked_NS_0.05	0.05	0.065	no damage
ked_NS_0.10	0.10	0.172	very light damage
Rnd_2	0.01	-	characterization
ked_NS_0.15	0.15	0.262	very light damage

Table 3 Set of acceleration input considered for testing the vault NT

Sequence	PGA [g]	PTA[g]	Damage
Rnd_3	0.01	-	characterization
ked_NS_0.10	0.10	0.173	very light damage
ked_NS_0.15	0.15	0.226	light damage
ked_NS_0.20	0.20	0.318	heavy damage
Rnd_4	0.01	-	characterization
ked_NS_0.20	0.25	0.398	collapse

Besides the real history accelerogram, a signal obtained from a multiple-frequency random excitation was given to the table (Rnd). Tables 2-3 show the set of inputs applied to the model WT and NT, respectively, indicating the values of PGA, PTA and the level of damage detected after each test.

4.2 Input acceleration

Tests were performed by applying the North-South component of the ground motion registered during the 21 May 2003 Keddara earthquake (ked_NS) along y direction.

The target acceleration time history is shown in Fig. 11(a). Figs. 11(b)-(c) show the target acceleration and the displacement response spectra, respectively, compared with the response spectra of the input actually measured on the table. The signal was normalised and rescaled to the site of the Citadel of Algiers according to the uniform hazard response spectrum (UHRS). Tests were performed at increasing value of Peak Ground Acceleration (PGA) of 0.05 g. The actual acceleration applied to the table, named Peak Table Acceleration (PTA), was measured with the accelerometer acc0. Besides the real history accelerogram, a signal obtained from a multiple-frequency random excitation was given to the table (Rnd).

Tables 2-3 show the set of inputs applied to the model WT and NT, respectively, indicating the values of PGA, PTA and the level of damage detected after each test.

4.3 Tests results

The seismic behaviour of the vault in both the configurations (WT and NT) was examined qualitatively by observing the main damage mechanisms, and quantitatively by analysing the records obtained by the 3DVision system (displacements and accelerations of the markers) and the accelerometers.

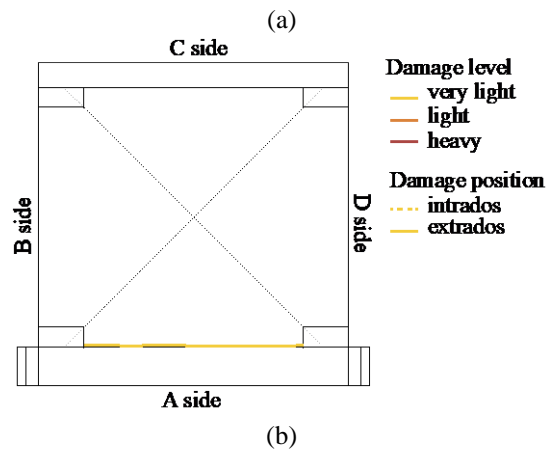


Fig. 12 Very light damage detected after the last test (PTA=0.262 g) on the vault WT: detailed view of the intersection between the vault and the wall A (a); top view of the crack pattern (b)

4.3.1 Damage and collapse mechanism

The development of damage was detected through qualitative visual inspections after each sequence of tests on both the configurations, WT and NT. It is worth to be noted that, the damage detected after the sequence of tests on the vault WT was very light (see Table 2) and in most of the case cracks were almost invisible to naked eyes. After the test ked_NS_0.15 (PTA = 0.262g), a very thin crack at the extrados of the vault WT, along the intersection between the vault profile and the arch spandrel on side A was just barely visible (Fig. 12(a)). A map of the detected crack pattern is shown in Fig. 12(b).

Concerning the tests on the vault NT, after the test ked_NS_0.10 (PTA = 0.173g), no damage was detected, excepting the very thin crack already identified after the previous tests on the vault WT. The damage slightly worsened during the test ked_NS_0.15 (PTA = 0.226g), with the development of a thin crack along the intersection between the vault and the wall C (Fig. 13(a)) and the widening of the crack between the vault and the arch spandrel (Fig. 13(b)-(c)). The damage level was light and caused by a physiological detachment between the vault and the walls that, as explained in Section 3.3, were not built together as a whole, but they were just juxtaposed. No damage, indeed, were detected at the level of the vault's supports, as illustrated in Fig. 13(d). After the following test sequence, ked_NS_0.20 (PTA=0.318 g), the gravity of damage increased (Fig. 14(a)-(b)) and a new very thin

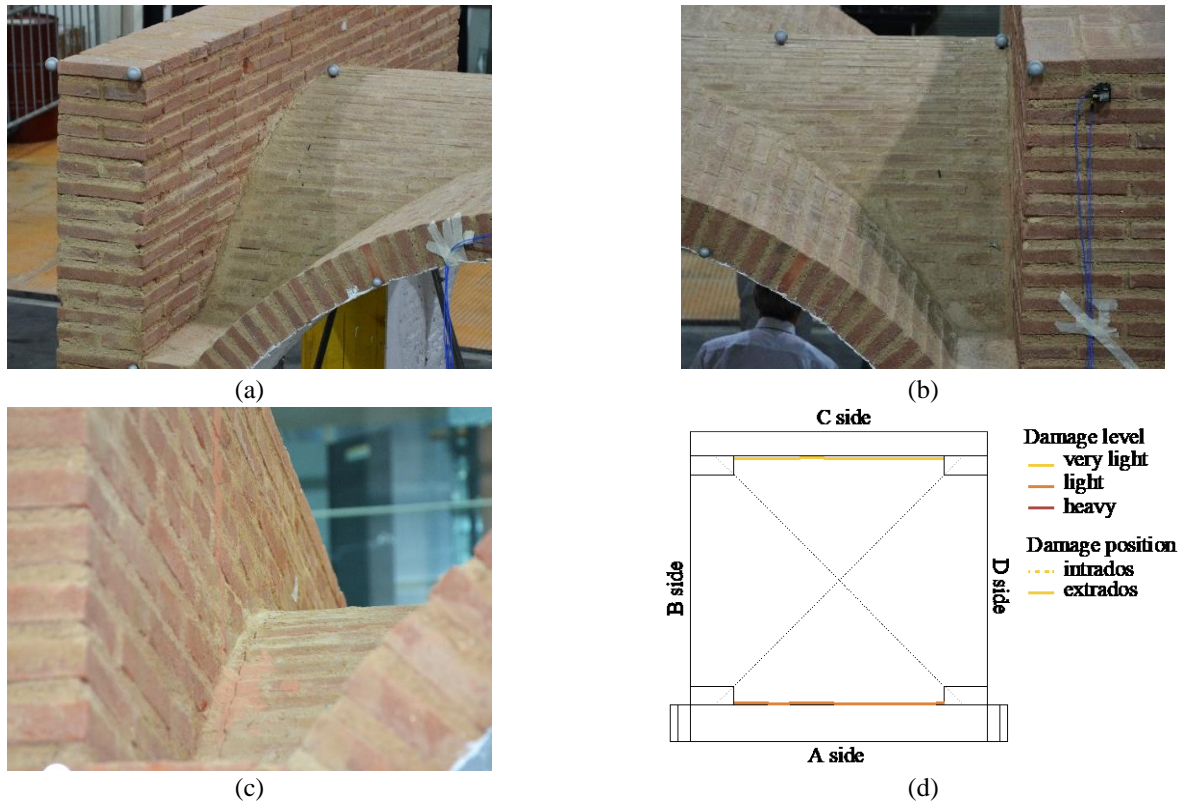


Fig. 13 Damage detected after the test *ked_NS_0.15* (PTA = 0.226g) on the vault NT: detailed views of the intersection between the vault and the wall C (a); the wall A (view from side B) (b); the wall A (view from side D) (c); and top view of the crack pattern (d)

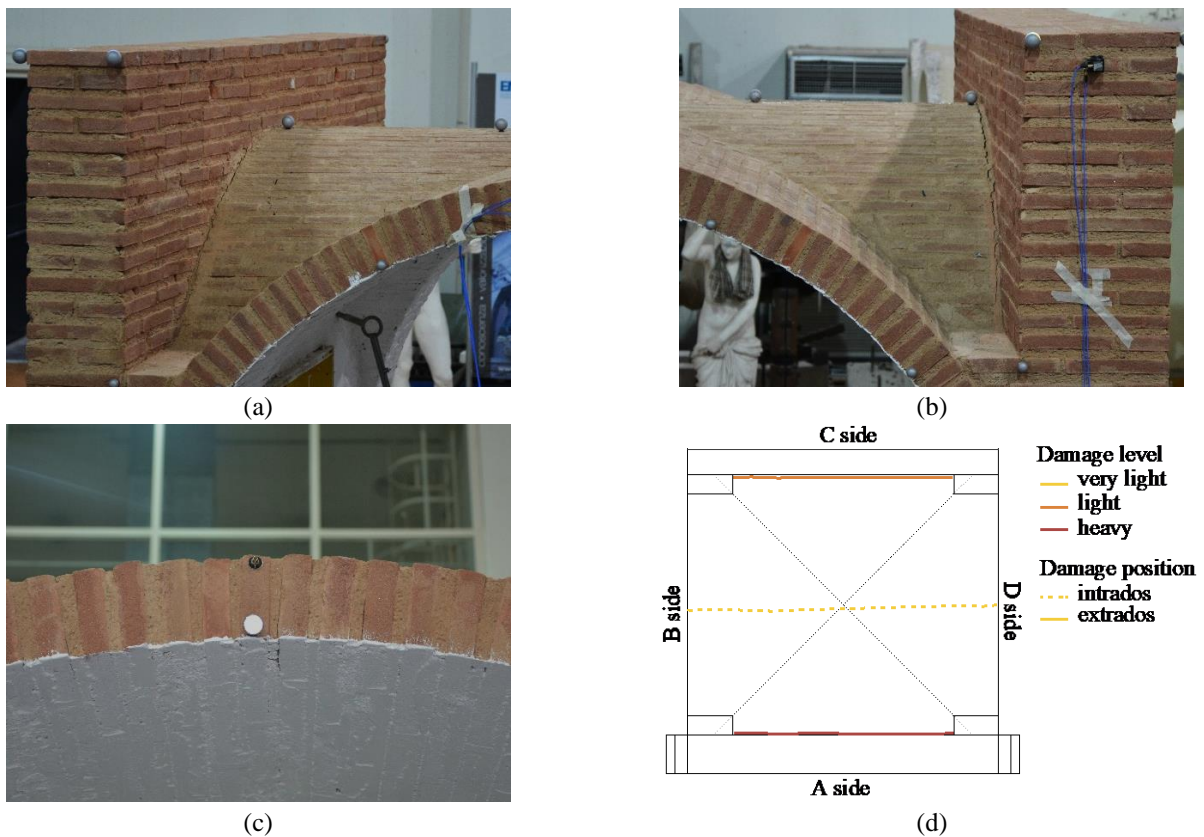


Fig. 14 Damage detected after the test *ked_NS_0.20* (PTA = 0.318g) on the vault NT: detailed views of the intersection between the vault and the wall C (a); the wall A (view from side B) (b); the middle of the vault's profile from side D (c); and top view of the crack pattern (d)

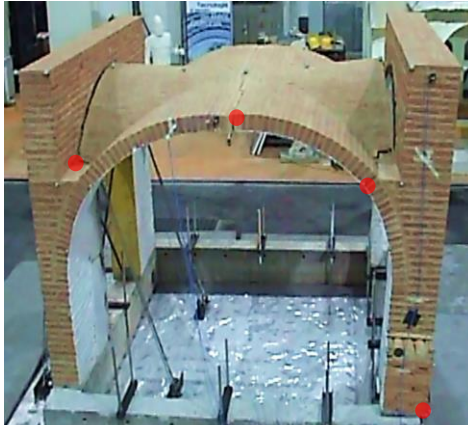


Fig. 15 Four-hinge collapse mechanism of the vault during the test *ked_NS_0.25* (PTA = 0.398g)

crack, parallel to the other two and passing through the vault's key, was detected (even though scarcely visible at naked eyes) at the intrados (Fig. 14(c)). This crack pattern revealed the activation of a three hinges mechanism of the vault. However, no damage was surveyed at the level of the vault's supports, as shown in Fig. 14(d). The collapse of the vault occurred abruptly during the test *ked_NS_0.25* (PTA=0.398 g). The failure mechanism was characterized by the overturning of the side A and the development of four hinges mechanism (three hinge on the vault and one hinge at the base of the abutments) along the x direction, as shown in Fig. 15. A sequence of images of the failure up to collapse is illustrated in Fig. 16.

The progress of damage throughout tests sequences was analysed not only by qualitative visual inspections but also



Fig. 16 Collapse mechanism of the vault NT for the seismic input of PTA=0.398 g, with the overturning of the side A and the development of a four-hinge mechanism on the vault

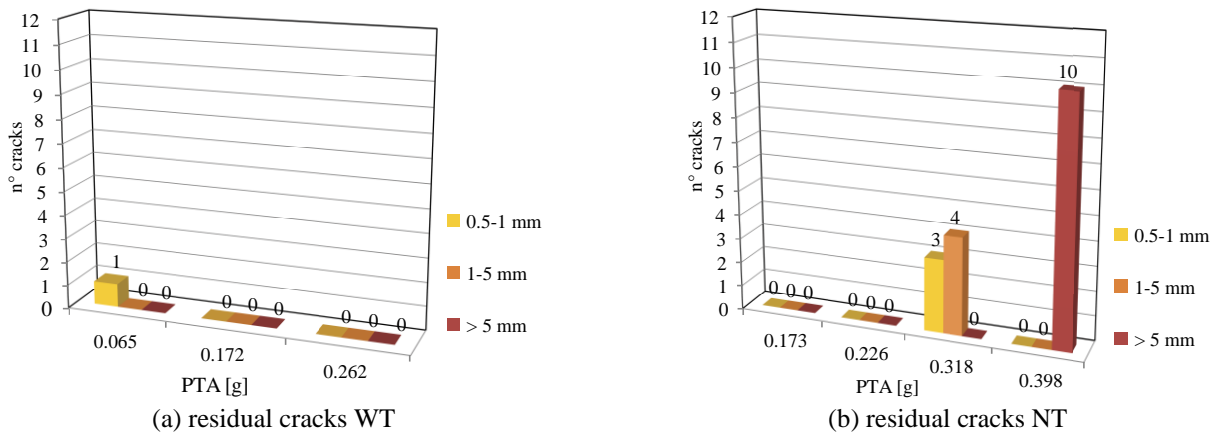


Fig. 17 Maximum number of cracks detected at the end of each test sequence in the vault WT (a) and NT (b)

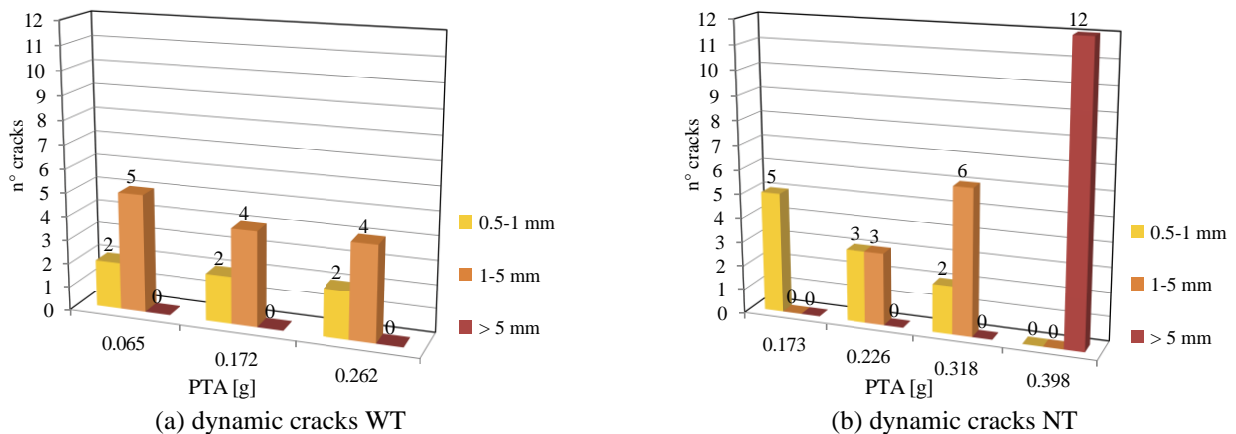


Fig. 18 Maximum number of cracks detected in dynamic condition in the vault WT (a) and NT (b)

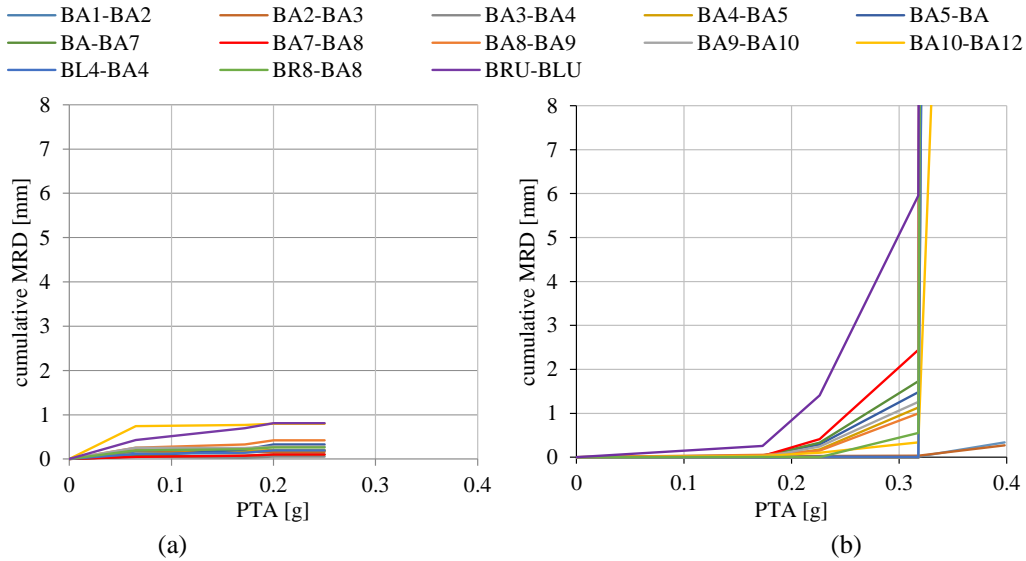


Fig. 19 Cumulative MRD results of tests in the vault WT (a) and NT (b)

by using the Markers Relative Displacements (MRDs) technique based on the 3DVision data analysis (Roselli *et al.* 2015). The NIR cameras allowed the detection of cracks that cause MRDs greater than 0.1-0.2 mm. Three classes of damage were defined on the basis of crack's thickness (0.5-1 mm, 1-5 mm, and higher than 5 mm), following damage thresholds described in the Italian regulations (OPCM 2017).

The number of residual cracks (openings) after each test sequence are shown in Figs. 17(a)-(b) for the vault WT and the vault NT, respectively. The maximum numbers of cracks that occurred throughout tests (dynamic cracks) are shown in Fig. 18(a) (vault WT) and Fig. 18(b) (vault NT).

For the vault WT, a light damage occurred as early as in the ked_NS_0.05 test. After the application of the input of PTA equal to 0.065 g, one crack 0.5-1 mm thick developed (Fig. 17(a)). However, in dynamic conditions, more than one crack (two openings 0.5-1 mm thick and five openings 1-5 mm thick) developed throughout the test, as shown in Fig. 18(a). With increasing the PTA (ked_NS_0.10 and ked_NS_0.15), no residual cracks were measured at the end of each test, while in dynamic conditions, there were two openings 0.5-1 mm thick and four openings 1-5 mm thick.

For the vault NT, no residual cracks were recorded up to the test with PTA equal to 0.318 g (ked_NS_0.20), when three openings 0.5-1 mm thick and four openings 1-5 mm thick occurred (Fig. 18(b)). Despite the lack of residual cracks, five cracks of thickness 0.5-1 mm opened during the test ked_NS_0.10 (PTA = 0.173 g), while three cracks of thickness 0.5-1 mm and three of thickness 1-5 mm opened during the test ked_NS_0.15 (PTA = 0.226 g). During the test of PTA equal to 0.318 g, two cracks of thickness 0.5-1 mm and six of thickness 1-5 mm developed.

Figs. 19(a)-(b) illustrate the cumulative MRDs, which provides the incremental growth of permanent deformations throughout the tests. In general, it can be observed that the vault WT was subjected to initial deformations, mainly localized at the level of the wooden logs (Fig. 19(a), BA10-BA12) and associated to an outward movements of the wall

A (Fig. 19(a), BRU-BLU). These small deformations occurred from the first test of PTA=0.065 g and remained basically constant throughout the three tests.

On the contrary, the vault NT exhibited the main deformations starting from the tests of PTA 0.226 g. As shown in Fig. 19(b), displacements are mainly associated to the increasing outward movement of wall A (BRU-BLU) and to the development of the hinges on the vault, in particular: BA7-BA8 (hinge at the level of one springing), BA-B A7 (hinge on the vault's crown), and BA4-BL4 (hinge at the level of the other springing).

4.3.2 In-plane and out-of-plane deformations

The markers displacement data provided by the 3D Vision system were used to calculate: i) the deformation of the vault in the xy plane (in-plane horizontal drift, Fig. 20(a)); ii) the in-plane shear deformation of the wall A in the yz plane (in-plane vertical drift, Fig. 20(b)); and iii) the displacement profile of the wall A in the xz plane (Fig. 20(c)).

The vault's in-plane shear deformation was analysed by calculating the relative displacements dy between the markers ALU-CRU (side B), and ARU-CLU (side D), as shown in Fig. 20(a). The trends of the drift dy/L , with L equal to the distance between the mid plane of the wall C and of the wall A are illustrated in Figs. 21(a)-(b) for the vault WT and NT, respectively.

In the model WT, the drift of side B was slightly bigger than of side D for the first two tests (PTA equal to 0.065 g and 0.172 g). In the last tests (PTA=0.262g), the in-plane response of the vault was almost symmetric, with a drift value of 0.07% in both sides. The same behaviour is observable in Fig. 22(a) that shows the vertical in-plane deformation of the wall A expressed in terms of the vertical drift dy/H , with H the distance between the markers ALU and AL1. The response was modestly asymmetric for the first two tests and symmetric for the last test. This small asymmetry was ascribable to local movements at the level of the abutments caused by settlements of the wooden logs,

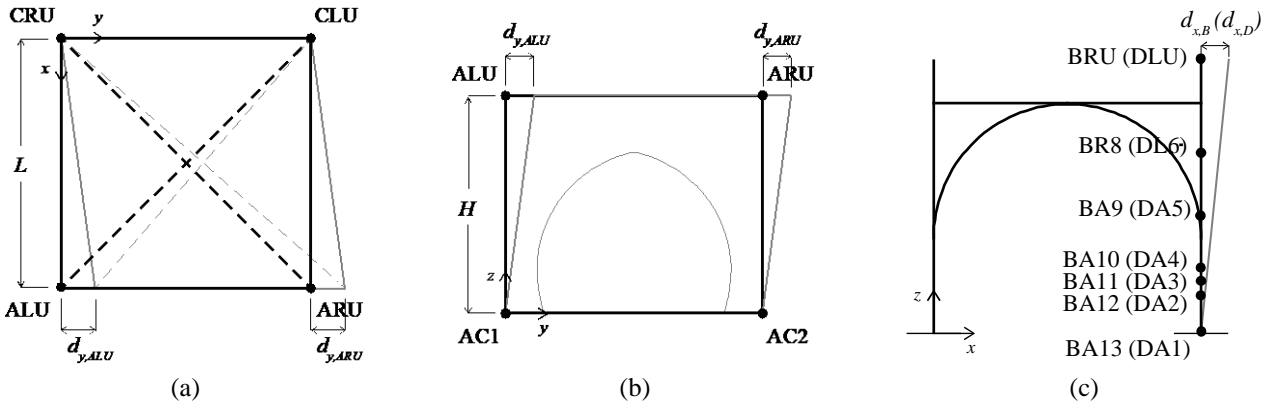


Fig. 20 (a) Horizontal in-plane deformation of the vault (xy plane, top view), (b) vertical in-plane shear of the wall A (yz plane), and (c) out-of-plane mechanism of the wall A (xz plane)

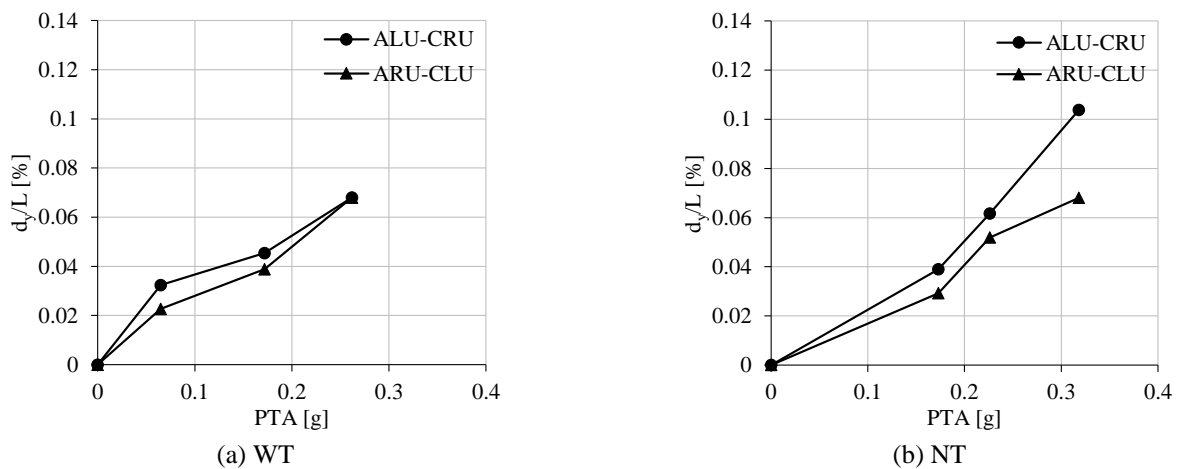


Fig. 21 Horizontal in-plane shear of the vault expressed in terms of displacement/vault's span ratio

which may not have been executed exactly the same way. The maximum in-plane vertical drift was equal to 0.08% (in both sides).

The model NT exhibited a higher asymmetry of the response between the sides B and D. During the test of $PTA=0.318$ g, the in-plane horizontal drift of side B (0.104%) was 50% bigger than the drift of side D (0.068%), as shown in Fig. 21(b). However, considering the in-plane vertical drift, the drift of side B was similar to the drift of side D for the first test, and it was smaller during the following tests, as shown in Fig. 22(b). The main reason was that the horizontal in-plane deformation was also affected by some torsional behaviour that increased the drift between ALU and CRU.

The displacement profiles of the wall A were created based on the relative displacement in x of the markers indicated in Fig. 22(c). Figs. 23(a)-(b) illustrate the displacement profiles for each test of the vault WT and the vault NT, respectively. The black curves indicate the displacement profile of side B, while the grey curves represent the displacement profile of side D.

The vault WT (Fig. 23(a)) exhibited an asymmetric response. In particular, the displacement measured on side B were higher than those on side D. It is worth noting that, however, this difference in drift is related to relatively small deformations produced by low PTA and may be affected by

any imperfections in stiffness between the two sides of the vault and any initial adjustment of the mock-up, especially at the level of the wooden logs where deformations were mainly concentrated. The higher value of displacement (0.9 mm) were measured in BA10 (just above the abutment) during the first test ($PTA=0.065$ g). This value was just 0.1 mm lower than the highest maximum displacement that was achieved by the marker BRU during the last test ($PTA=0.265$ g).

On side D, displacements show a more regular profile, increasing with the markers' coordinate z and with the seismic input.

The displacement profiles obtained by the three tests of the vault NT (Fig. 23(b)) present a symmetric behaviour on average. The maximum displacement achieved before the collapse ($PTA=0.318$ g) was of 5.2 mm and measured in BLU. This value was four times higher than that measured in the previous test ($PTA=0.226$ g).

The deformed shapes of the vault NT in both the xy and the xz plane are shown in Figs. 24(a)-(b), respectively.

5. Dynamic identification

The analysis of the dynamic identification tests allowed determining the modal frequencies and the main dynamic

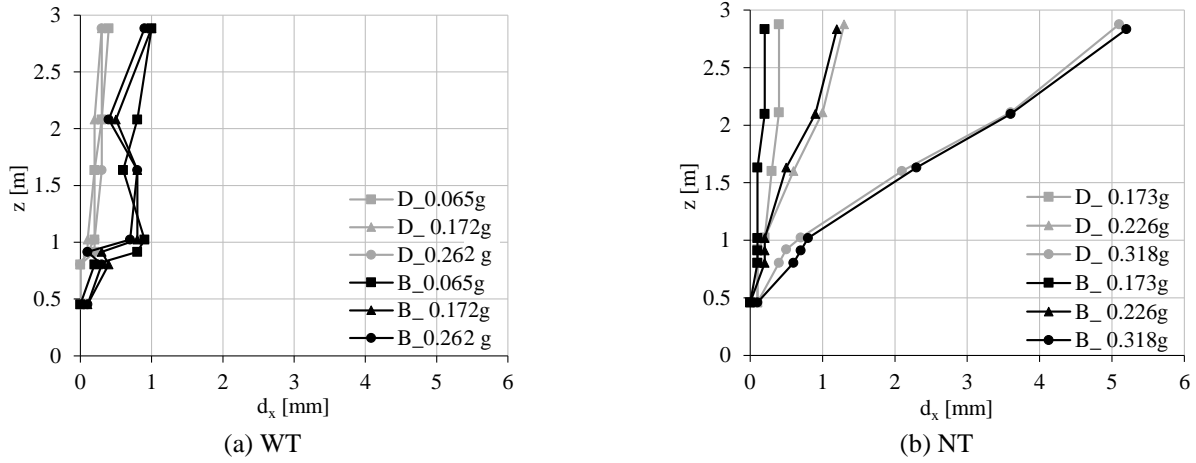


Fig. 23 Displacement profiles of the wall A on both sides B and D

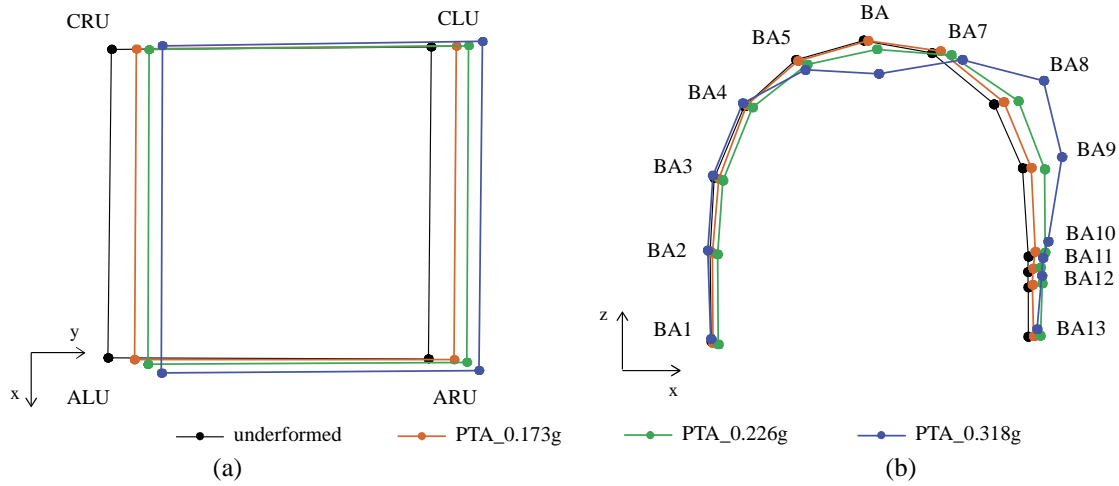


Fig. 24 Deformed shapes of the vault NT: (a) horizontal in-plane deformed shapes from the vault's top view and (b) deformed shapes of the vault from side B

parameters of the structure through the application of the Frequency Response Function (FRF). In particular, the dynamic of the wall A subject to overturning was analysed.

5.1 Experimental modal analysis

The dynamic behaviour of the vault WT and NT was examined by analysing the data acquired during the four random white noise tests before and after the seismic tests. Velocity and acceleration of each marker were estimated by numerical differentiation of the displacement data, as well as the estimation of the dynamic properties of the vault based on the input and output displacement Frequency Response Function (FRF)d-d (Transmissibility Function) of each marker with respect the reference point AC2 (see Fig. 11). The data processing procedure for the first and second derivatives of the displacement data was based on the Savitzky-Golay (SG) smoothing filter, with a six order fitting polynomial degree and 0.1 sec moving window width.

The graphs in Fig. 25 show the Transmissibility Function (FRF)d-d of the markers at the points ALU and ARU (top of the wall A), in the x and y direction, during the

test Rnd_1 (vault WT). The graphs in Fig. 26 show the (FRF)d-d at the same markers during the test Rnd_4 (vault NT). The graphs show also the Synthetic FRF (S_FRF) obtained using a 3DOF modal model, calculated as Eq. (1).

$$FRF_{Synt}(f) = \sum_{r=1}^N H_r \cdot \left[\frac{(1 - \lambda_r^2)}{(1 - \lambda_r^2)^2 + (2\zeta_r \lambda_r)^2} - i \frac{2\zeta_r \lambda_r}{(1 - \lambda_r^2)^2 + (2\zeta_r \lambda_r)^2} \right] \quad (1)$$

The dynamic models of the wall A are described by the parameters in Tables 4-5, where f_r are the first three critical frequencies ($r=1, 2, 3$), S_FRF_r are the corresponding peak values of the Synthetic Transmissibility Function, ζ_r are the -3dB estimated a-dimensional damping, H_r are the Modal Constants, and $\lambda_r = f/f_r$.

The Power Spectral Density (PSD) of the displacement data describes their frequency composition in terms of the Root Mean Square (RMS) value in the frequency domain. Therefore, the integrated PSD within the frequency range describes the energy growth at each frequency, and the steps at the first three resonant frequencies are proportional

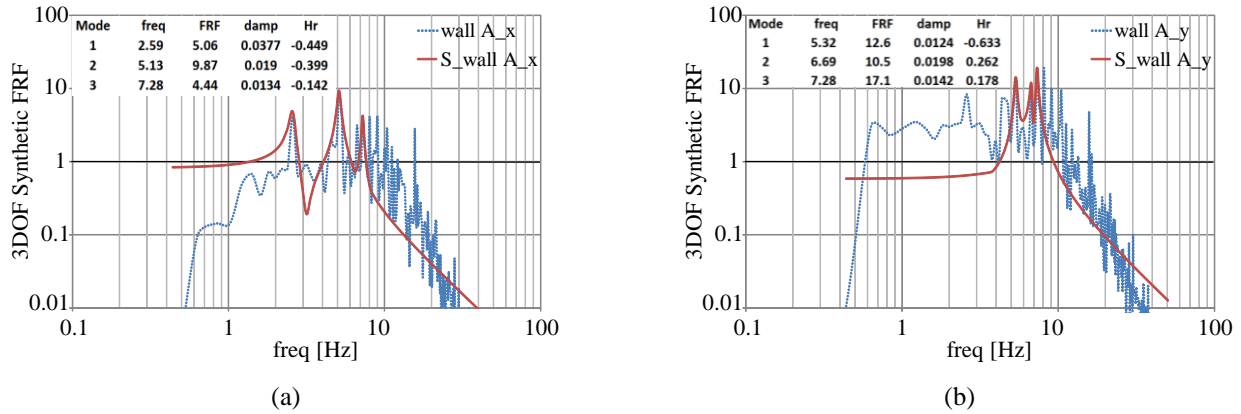


Fig. 25 Test Rnd_1 in the vault WT, Displacement input-Displacement Output Transmissibility function (FRF)_{d-d} of the wall A in (a) x and (b) y direction

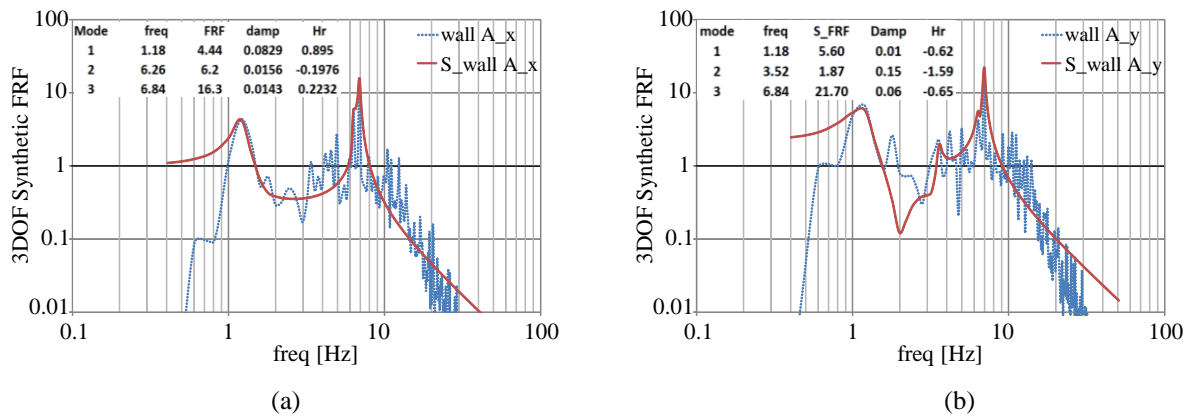


Fig. 26 Test Rnd_4 in the vault NT, Displacement input-Displacement Output Transmissibility function (FRF)_{d-d} of the wall A in (a) x and (b) y direction

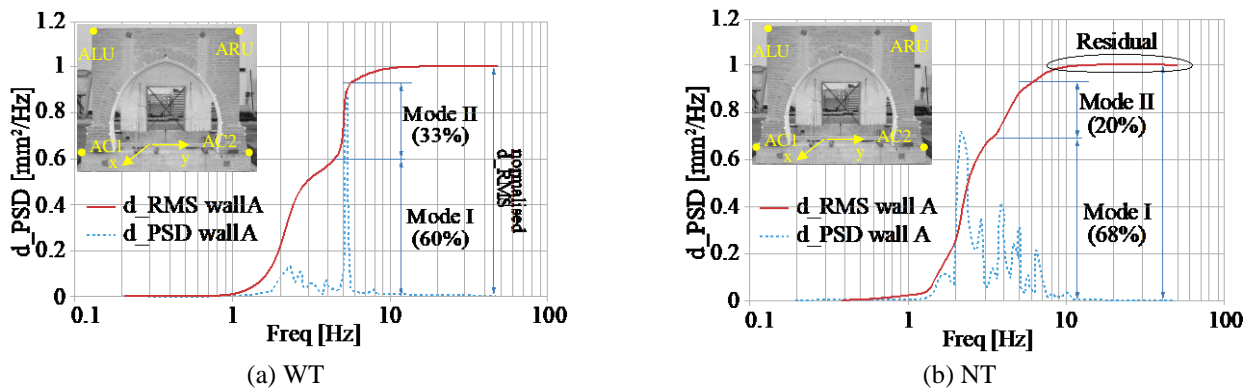


Fig. 27 Power Spectral Density of the displacement at the wall A Control Points and associated frequency contribution to the Root Main Square displacement calculated for (a) test Rnd_1 (WT) and (b) Test Rnd_4 (NT)

to the modal participation coefficients. Figs. 27(a)-(b) show the PSD of the displacements at the wall A control points (ALU and ARU at the top, AC1 and AC2 at the bottom) and the associated frequency contributions to the RMS value of the displacement time histories. This allows estimating the modal participation factors, and consequently the modal mass participation to calculate the spectral acceleration activating the collapse kinematics of the wall (De Canio *et al.* 2015).

When comparing the frequencies obtained from the test on the vault WT and those on the vault NT, it can be observed that, although the longitudinal steel bars should constitute a constraint in x, their removal cause a reduction of the frequency which is higher in y (mode 1, from 5.32 Hz to 1.18 Hz) than in x (mode 1, from 2.59 Hz to 1.18 Hz). The main reason can be ascribable to a not negligible flexional stiffness of the bars that also inhibited the activation of the in-plane mechanism of the vault. However,

Table 4 Test Rnd_1 (WT), dynamic model of the wall A

r	f_r	S_{FRF_r}	ζ_r	Hr
1	2.59	5.06	0.04	-0.45
2	5.13	9.87	0.02	-0.40
3	7.28	4.44	0.01	-0.14

when the longitudinal bars were removed, the mechanism in x prevailed.

Considering the FRF results of the vault WT (see Fig. 25), the first and the second modes correspond to the modes 1 and 2 in x, with a frequency of 2.59 Hz and 5.13 Hz, respectively. The second mode's frequency value was close to the frequency of the mode 1 in y, equal to 5.32 Hz.

The highest frequency had an equivalent value (7.28 Hz) in both the directions. Analysing the FRF results of the vault NT (see Fig. 26), it can be observed that the first mode frequency of 1.18 Hz is equal in both directions. The second mode was the mode 2 in y (3.52 Hz) and the third mode is the mode 2 in x (6.26 Hz).

6. Conclusions

The paper investigated the dynamic response on a shaking table of a brick masonry mock-up of a cross vault simulating one of the cross vault in the Mosque of Dey in Algeri. The tests were performed by applying the NS component of the Keddara earthquake along y direction. The value of the PGA was progressively increased by 0.05g. Two different setup were tested: in the first case, the vault was equipped with a couple of steel bars at the top of the walls (vault WT) and in the second, the bars were removed (vault NT). The use of a 3D optical system combined with displacement data processing permitted an accurate understanding of the damage mechanism and the dynamic behaviour of the mock-up during the tests. The results were discussed in terms of development of damage using the Markers Relative Displacements (MRDs) technique based on the 3DVision data analysis, displacements/deformations, and collapse mechanism. Moreover, an experimental modal analysis allowed to determine the modal participant coefficients concerning both vault WT and NT. Conclusions can be summarized as follows.

- The vault NT collapsed during the last test with a PGA equal to 0.25 g corresponding to a peak table acceleration equal to 0.398 g. The main mechanism of collapse was the out-of-plane response of the side A of the model (wall A overturning) and the development of a four-hinge mechanism of the vault.
- In the vault WT, the maximum cumulative MRD were measured between markers BA10 and BA12 above the abutments (0.79 mm) and between markers BLU and BRU at the top of the wall A and the wall C (0.81 mm).
- In the vault NT, the maximum cumulative MRD (excluding the test at collapse) were measured between markers BA7 and BA8 at the level of the formation of an arch's hinge (2.44 mm) and between markers BLU and BRU at the top of the wall A and the wall C (5.96 mm).

Table 5 Test Rnd_4 (NT), dynamic model of the wall A

r	f_r	S_{FRF_r}	ζ_r	Hr
1	1.18	4.44	0.08	0.89
2	6.26	6.2	0.01	-0.2
3	6.84	16.5	0.01	0.22

•In the vault NT, the in-plane deformation was reasonably symmetric because of the presence of the longitudinal steel constraints at the top of the model; however, modest difference between the relative displacement dy of side B and side D occurred because of local settlements of the wooden logs at the abutments.

•In the vault NT, the in-plane deformation was not symmetric mainly because of the prevailing of some torsional effects.

The absence of the longitudinal steel bars led to a drop of the stiffness not just in x, but also in y direction. The frequency of the first mode in x decreased from 2.59 Hz to 1.18 Hz, while the first mode in y decreased from 5.32 Hz to 1.18 Hz. This result is ascribable by a not negligible flexural stiffness of the bars that constrained the development of an in-plane deformation of the vault WT.

Acknowledgments

This experimental research activity received funding from the European Community's Seventh Framework Programme (FP7/2007–2013) under Grant agreement No. 244229 (www.perpetuate.eu). The authors also acknowledge the enterprise "Il Cenacolo s.r.l." for the help and the support in the vault's mock-up building.

References

- Abdessemed-Foufa, A. (2012), "Visual screening for a potential evaluation of seismic vulnerability of historical building: Palace of the Dey (Citadel of Algiers)", *WIT Transac. Built Envir.*, **123**, 119-123.
- Abdessemed Foufa, A., Terki, Y. and Benouar, D. (2015), *Case Study: Local Seismic Culture in Vernacular Architecture in Algeria*, in *Seismic Retrofitting: Learning from Vernacular Architecture*, CRC Press, London, U.K.
- Atamturktur, S., Pavic, A., Reynolds, P. and Boothby, T. (2009), "Full-scale modal testing of vaulted gothic churches: lessons learned", *Exp. Techniq.*, **33**(4), 65-74. <https://doi.org/10.1111/j.1747-1567.2009.00523.x>.
- Boothby, T.E. (2001), "Analysis of masonry arches and vaults", *Prog. Struct. Eng. Mater.*, **3**(3), 246-256. <https://doi.org/10.1002/pse.84>.
- Calvo Barentin, C., Van Mele, T. and Block, P. (2017), "Robotically controlled scale-model testing of masonry vault collapse", *Meccanica*, **53**(7), 1917-1929. <https://doi.org/10.1007/s11012-017-0762-6>.
- Cangi, G. (2005), *Manuale Del Recupero Strutturale e Antisismico*, Manuali per l'edilizia, Italy.
- Cattari, S., Resemini, S. and Lagomarsino, S. (2008), "Modelling of vaults as equivalent diaphragms in 3D seismic analysis of masonry buildings", *Proceedings of the Sixth International Conference on Structural Analysis of Historic Construction*, Bath, U.K., July.

- Ceradini, V. (1996), "Modelli sperimentali di volte", In *Atti del Convegno Nazionale La Meccanica delle Murature tra Teoria e Progetto*, Messina, Italy, September.
- Conte, C., Rainieri, C., Aiello, M.A. and Fabbrocino, G. (2011), "On-site assessment of masonry vaults: Dynamic tests and numerical analysis", *Geofizika*, **28**(1), 127-134. <https://hrcak.srce.hr/70837>.
- De Canio, G., de Felice, G., De Santis, S., Giocoli, A., Mongelli, M., Paolacci, F. and Roselli, I. (2016), "Passive 3D motion optical data in shaking table tests of a SRG-reinforced masonry wall", *Earthq. Struct.*, **40**(1), 53-71. <http://dx.doi.org/10.12989/eas.2016.10.1.053>.
- De Canio, G., Mongelli, M. and Roselli, I. (2013), "3D motion capture application to seismic tests at ENEA Casaccia research center: 3Dvision system and DySCo virtual lab", *WIT Trans. Built Environ.*, **134**, 803-814.
- De Canio, G., Mongelli, M., Tatì, A., Roselli, I., Giocoli, A. and Rinaldis, D. (2015), "Structural monitoring of the columns at the Cathedral of Orvieto", *Proceedings of 7th International Conference on Structural Health Monitoring of Intelligent Infrastructure (SHMII-7)*, Turin, Italy, July.
- Gaetani, A., Monti, G., Lourenço, P.B. and Marcari, G. (2016), "Design and analysis of cross vaults along history", *Int. J. Arch. Heritage*, **10**(7), 841-856. <https://doi.org/10.1080/15583058.2015.1132020>.
- Giamundo, V., Lignola, G.P., Maddaloni, G., Balsamo, A., Prota, A. and Manfredi, G. (2015), "Experimental investigation of the seismic performances of IMG reinforcement on curved masonry elements", *Compos. Part B: Eng.*, **70**, 53-63. <https://doi.org/10.1016/j.compositesb.2014.10.039>.
- Giresini, L., Sassu, M., Butenweg, C., Alecci, V. and De Stefano, M. (2017), "Vault macro-element with equivalent trusses in global seismic analyses", *Earthq. Struct.*, **12**(4), 409-423. <http://doi.org/10.12989/eas.2017.12.4.409>.
- Gurrieri, F. (1999), *Manuale Per la Riabilitazione e Ricostruzione Post-Sismica Degli Edifici*, DEI, Rome, Italy.
- Huerta, S. (2004), Arcos, *Bóvedas y Cúpulas. Geometría y Equilibrio en el Cálculo Tradicional de Estructuras de Fábrica*, Institute Juan Herrera, Madrid, Spain.
- Huerta, S. (2008), "The analysis of masonry architecture: a historical approach", *Arch. Sci. Rev.*, **51**(4), 297-328. <https://doi.org/10.3763/asre.2008.5136>.
- Lagomarsino, S., Penna, A., Galasco, A. and Cattari, S. (2013), "TREMURI program: An equivalent frame model for the nonlinear seismic analysis of masonry buildings", *Eng. Struct.*, **56**, 1787-1799. <https://doi.org/10.1016/j.engstruct.2013.08.002>.
- OPCM (2017), "Misure per il ripristino con miglioramento sismico e la ricostruzione di immobili ad uso abitativo gravemente danneggiati o distrutti dagli eventi sismici verificatisi a far data dal 24 agosto", Report No. 143, Gazzetta Ufficiale, Rome, Italy.
- Quinonez, A., Zessin, J., Nutzel, A. and Ochsendorf, J. (2010), "Small-scale models for testing masonry structures", *Adv. Mater. Res.*, **133**, 497-502. <https://doi.org/10.4028/www.scientific.net/AMR.133-134.497>.
- Ramaglia, G., Lignola, G.P. and Prota, A. (2016), "Collapse analysis of slender masonry barrel vaults", *Eng. Struct.*, **117**(15), 86-100. <https://doi.org/10.1016/j.engstruct.2016.03.016>.
- Roselli, I., Mongelli, M., Tatì, A. and De Canio, G. (2015), "Analysis of 3D motion data from shaking table tests on a scaled model of Hagia Irene", *Key Eng. Mater.*, **624**, 66-73. <https://doi.org/10.4028/www.scientific.net/KEM.624.66>.
- Rossi, M., Calderini, C. and Lagomarsino, S. (2015), "Seismic Response of Masonry Cross vaults: Experimental Tests and Definition of a Macroelement Model", *Atti Del 16th Convegno ANIDIS, L'Aquila*, Italy, September.
- Rossi, M., Calderini, C. and Lagomarsino, S. (2016), "Experimental testing of the seismic in-plane displacement capacity of masonry cross vaults through a scale model", *Bull. Earq. Eng.*, **14**(1), 261-281. <https://doi.org/10.1007/s10518-015-9815-1>.
- Rossi, M., Calvo Barentin, C., Van Mele, T. and Block, P. (2017), "Experimental study on the behaviour of masonry pavilion vaults on spreading supports", *Struct.*, **11**, 110-120. <https://doi.org/10.1016/j.istruc.2017.04.008>.
- Shapiro, E.E. (2012), "Collapse mechanisms of small-scale unreinforced masonry vaults", MsC Dissertation, Massachusetts Institute of Technology, Massachusetts, U.S.A.
- Theodossopoulos, D., Makoond, N. and Akl, L. (2016), "The effect of boundary conditions on the behaviour of pointed masonry barrel vaults: late gothic cases in Scotland", *Open Constr. Build. Tech. J.*, **10**(2), 274-292. <http://10.2174/1874836801610010274>.
- Theodossopoulos, D., Sinha, B.P., Usmani, A S. and Macdonald, A.J. (2002), "Assessment of the structural response of masonry cross vaults", *Strain*, **38**(3), 119-127. <https://doi.org/10.1046/j.0039-2103.2002.00021.x>.
- Tralli, A., Alessandri, C. and Milani, G. (2014), "Computational methods for masonry vaults: a review of recent results", *Open Civil Eng. J.*, **8**(1), 272-287. <http://hdl.handle.net/11311/883050>.
- Van Mele, T., McInerney, J., DeJong, M. and Block, P. (2012), "Physical and Computational Discrete Modelling of Masonry Vault Collapse", *Proceedings of 8th International Conference on Structural Analysis of Historical Constructions*, Wroclaw, Poland, October.

CC